Mecánica Computacional Vol. XXI, pp. 2606–2621
S. R. Idelsohn, V. E. Sonzogni and A. Cardona (Eds.)
Santa Fe–Paraná, Argentina, October 2002

FATIGUE ANALYSIS THROUGH FINITE ELEMENT MODELS FOR PAPER SUCTION ROLLS

Mario Vega[*], Mario Razeto[†], Emilio Dufeu[†] and Alvaro Hillerns[†]

[*] CADETECH S.A.
Serrano 551, Oficina 208
Concepción, Chile
e-mail: cadetech@surnet.cl, web page: http://www.cadetech.cl

[†] Departamento de Ingeniería Mecánica
Universidad de Concepción
Concepción, Chile
e-mail: mrazeto@udec.cl, web page: http://www.dim.udec.cl

Key words: paper, suction roll, fatigue, finite elements, reliability

Abstract*: This paper focuses on the application of fatigue life prediction to paper suction rolls. The procedure was developed to perform failure analysis requested by a local paper manufacturer.*
A numerical method must be employed to determine stresses, due to both the complex loading and the stress concentrators induced by perforations on the shell. The finite element method was used. A two-model approach was chosen. A global model of the roll was constructed using shell elements and taking into account the orthotropic behaviour induced by the perforations. A detailed plane stress model was used to compute the stress concentrators around perforations. Fatigue analysis was performed. Multi-axial stress concentration factors were determined from stress results. The high perforated area on the shell made it necessary to introduce an area reduction factor usually not accounted for in fatigue analysis. Reliability of the roll was determined taking into account the high number of notches.
The convergence of the stress solution was investigated, via successive refinement of the mesh. Automatic refinement tools are not suitable to this problem given the amount of stress concentrators.
Results from analysis indicate that the two mayor factors affecting the predicted life of the roll are the stress concentrators around the perforations and the loss of reliability due to the amount of these notches. Hence, the accuracy of stress results from the finite element models is particularly important in this problem.

1 INTRODUCTION

This paper focuses on the application of the finite element method to a particular fatigue problem with complex geometry and loading.

Suction rolls are used in the paper industry to dry and compress the paper. Two rolls are pressed against each other, making contact in the n ip area. In order to dry the paper, suction rolls are perforated and vacuum is generated on the inside. These perforations generate stress concentrations.

Contact pressure on the nip area generates high circumferential stresses, which must be evaluated via a numerical method. This is also necessary for the perforations stress concentrations. The finite element method was applied.

Since rolls rotate, the nip area changes in time and therefore loads are cyclic. Suction rolls are particularly prone to fatigue cracking because the multiple perforations imply multiple possible crack initiation sites. This characteristic justifies a stochastic life prediction approach, taking into account the variability of the fatigue life for each notch.

2 TWO-MODEL FINITE ELEMENT STRESS ANALYSIS

Suction rolls have a perforated surface in the range of 20-40 %. This translates into thousands of stress concentrators. Thus, meshing the actual geometry is impractical given current computational resources. Instead, a two-model approach was chosen. The roll was modelled with shell elements assuming a continuum mechanics behaviour. Stress concentrators on the perforations were evaluated via a plane stress model, using results from the shell model of the roll as boundary conditions.

Care was taken to account for the change in the elastic moduli introduced by the perforations array. The perforated shell becomes slightly anisotropic. Equivalent elastic moduli in the longitudinal and circumferential directions were determined.

2.1 Equivalent elastic moduli for bending and traction

Results from previous suction rolls analysis indicate that the cylinder material is mainly subject to stresses from longitudinal and circumferential bending. Therefore, the equivalent elastic modulus for the longitudinal axis was determined by evaluating the displacements on a perforated coupon subject to axial traction. The modulus for the circumferential axis was by determined evaluating the displacements on a coupon subject to bending loads (see Fig. 1 (a) and 1(b)). The results indicate a 48% decrease in the elastic modulus for the longitudinal axis and a 51% decrease in the elastic modulus for the circumferential axis, compared to the modulus of the base material.

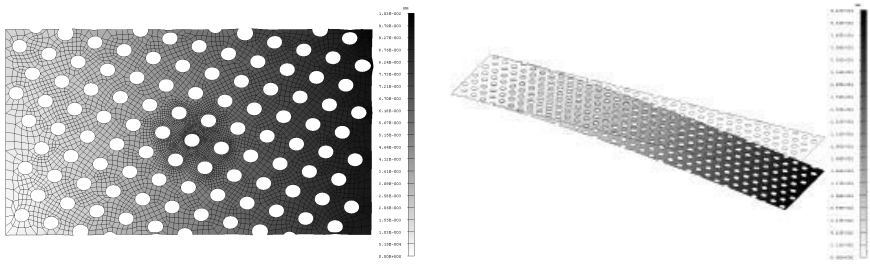

(a) Longitudinal axis, traction load (b) Circumferential axis, bending load

Figure 1: Finite element models used to determine equivalent elastic moduli

2.2 Finite element model of roll shell

A finite element model of the roll was constructed. The roll cylinder was modelled using 4432 second order shell elements. Orthotropic behaviour was specified, using the previously determined equivalent elastic moduli for the longitudinal and circumferential local axes. The end supports were modelled using 3344 second order tetrahedral elements. The finite element mesh for the roll assembly is shown in Fig. 2.

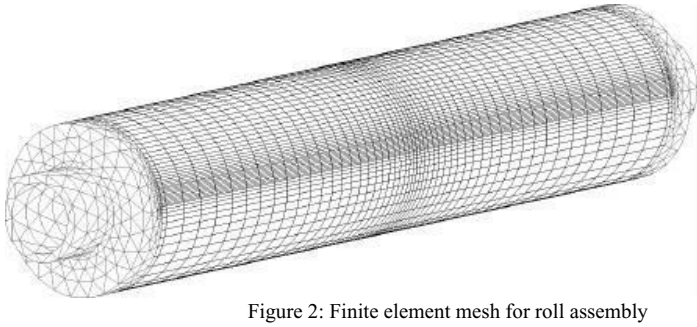

Figure 2: Finite element mesh for roll assembly

Although in reality the roll rotates and therefore the loads on a given point on the cylinder surface vary in time, it is possible to perform the fatigue analysis with just one static loadcase given the low rotation speed (30 rpm).

The applied loads are summarised in table 1 and shown in Fig.3. Since the length of the roll cylinder is 5.35 m, the load on Nip1 alone is more than twice the weight of the roll assembly.

Table 1: Applied loads for roll cylinder

Load	Value
Nip 1	90 kN/m
Nip 2	70 kN/m
Seal 1	0.5 bar
Seal 2	0.5 bar
Vacuum 1	0.7 bar
Vacuum 2	0.4 bar
Weight	225 kN

The deformed shape of the roll cylinder mid-section is shown in Fig.3. The highest deformation takes place in the nip 1 area, resulting in high circumferential stresses, as shown in Fig. 4 (a). Due to the bending direction, the highest traction stresses are on the inside surface or the roll. Also, the stresses are maximum at the longitud inal mid-section of the roll. The stress state in this area was assessed through the computation of the maximum principal stresses and its directions, shown in Fig. 6 (b). The fact that the principal directions match the circumferential and longitudinal di rections determines a rather simple load case to be applied to the detailed plane stress finite element model, in order to determine the stress concentrations.

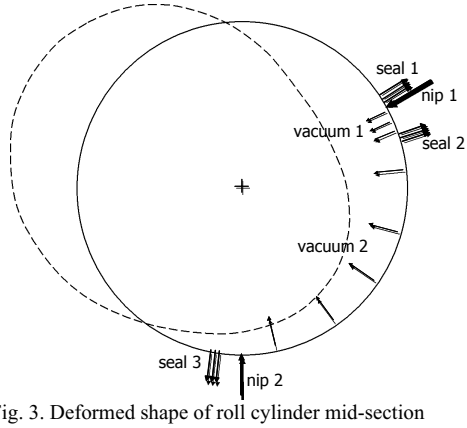

Fig. 3. Deformed shape of roll cylinder mid-section

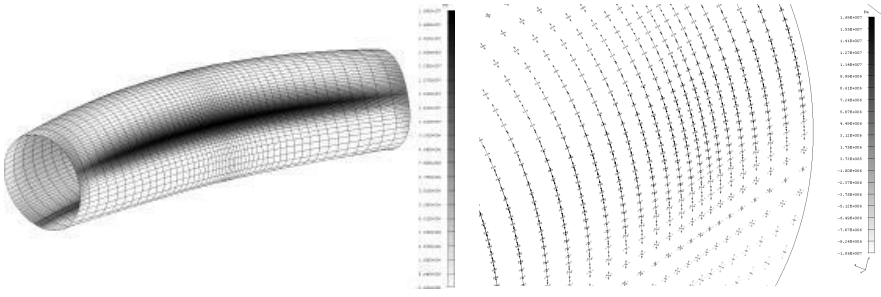

(a) Maximum principal stress contours (b) Maximum principal stresses

Fig. 4. Results of the finite element model of the roll assembly

2.3 Plane stress finite element model to determine stress concentrations

The abovementioned simplifications, namely plane stress conditions on the inside of the roll and a simple static load case, allow the computation of the stress state around the array of perforations via a model shown in Fig. 5. The input distributed loads S_θ and S_z are imported from the results of the finite elements model of the roll.

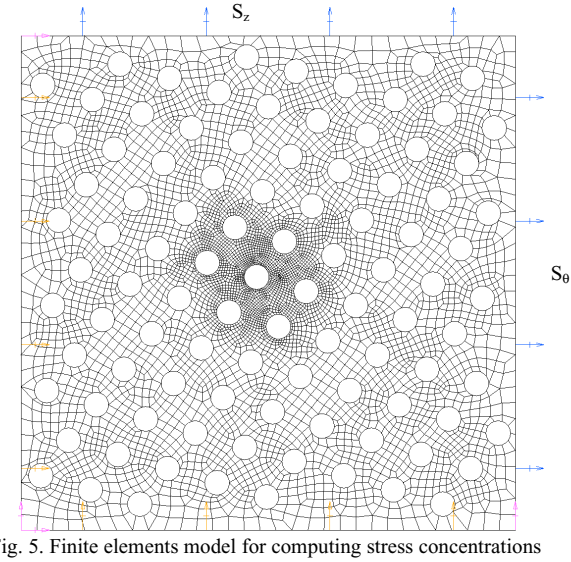

Fig. 5. Finite elements model for computing stress concentrations

3 FATIGUE ANALYSIS

3.1 Multi-axial fatigue analysis

Stress results from the shell finite elements model of the roll indicate a bi-axial stress state in the critical area. Thus, multi-axial stress analysis was considered. Goodman's relation may be written [1] in terms of an equivalent cyclic stress amplitude $\sigma_{m,e}$ and an equivalent mean stress $\sigma_{m,e}$, as follows.

$$\frac{1}{N} = \frac{\sigma_{m,e}}{\sigma_r} + K_{f,e}\frac{\sigma_{a,e}}{\sigma_f} \tag{1}$$

The equivalent cyclic stress amplitude, computed using von Mises correlation for a bi-axial stress state, equals

$$\sigma_{a,e} = \sqrt{\frac{1}{2}\left[(\sigma_{a1} - \sigma_{a2})^2 + {\sigma_{a1}}^2 + {\sigma_{a2}}^2\right]} \tag{2}$$

The equivalent mean stress using von Mises correlation yields

$$\sigma_{m,e} = \sqrt{\frac{1}{2}\left[(\sigma_{m1} - \sigma_{m2})^2 + {\sigma_{m1}}^2 + {\sigma_{m2}}^2\right]} \tag{3}$$

Equation 3 disregards the fact that a mean tension stress decreases fatigue life whereas a mean compressive stress extends it. This phenomenon was included in Sines' empirical equation [2], which was later simplified by Fuchs and Stephens [3] as follows

$$\sigma_{m,e} = \sigma_{m1} + \sigma_{m2} \tag{4}$$

To consider stress concentrators factors, each stress component must be multiplied by a respective concentrator factor, as proposed by Zahavi[1]. The equivalent cyclic stress amplitude taking into account stress notch factors in a general form is

$$K_t\sigma_{a,e} = \sqrt{\frac{1}{2}\left[(K_{t\theta}\sigma_{a\theta} - K_{tz}\sigma_{az})^2 + {K_{t\theta}\sigma_{a\theta}}^2 + {K_{tz}\sigma_{az}}^2 + {K_{t\theta z}6\tau_{\theta z}}^2\right]} \tag{5}$$

The theoretical stress concentrators are given by

$$K_t = \frac{theoretical\ peak\ stress\ in\ notched\ specimen}{nominal\ stress\ in\ notched\ specimen}$$

The computation of the theoretical stress concentration factors via the plane stress finite element model appears to be straightforward. Nevertheless, the high perforated area (30%) requires to separate the effects of the decrease in resisting area and the stress concentrator due to notches. Regularly both effects are accounted for in the stress concentrator factor, since the actual decrease in area introduced by most single notches is negligible. The stress factor due to area reduction is

$$K_a = \frac{A_0 - A_p}{A_0} \tag{6}$$

and the theoretical stress concentrator due to the notch is

$$K_t = \frac{K_{fem}}{K_a} \tag{7}$$

The area reduction and notch stress factors must to be determined individually because they affect fatigue life in a different manner. The area reduction factor must be applied to all stress results from the (not perforated) shell finite element model of the roll, in order to obtain true nominal stresses. Therefore, the area reduction factor affects both the mean and cyclic terms of equation 1. The theoretical stress concentrator due to the notch is used to compute the equivalent fatigue notch factor using Neubert's formula [4].

$$K_f = 1 + \frac{K_t - 1}{1 + \sqrt{\frac{a}{r}}} \tag{8}$$

where r is the notch radius and a is a material property constant. In this particular case r=2 mm and according to data from Grover [5] a=0.2 mm for a steel with 680 MPa ultimate strength.

Equation [7] estimates the sensitivity of the fatigue life to a certain notch stress concentrator for a given material and notch radius. A higher stress gradient (higher $K_{n,t}$) results in a lower fatigue life sensitivity, thus equation 7 yields a lower K_f, as would have been the case if a single stress concentrator factor had been used.

Equations 1 through 7 define the fatigue analysis problem for a bi-axial stress state and may be applied to the paper roll problem. In spite of that, care must be taken in the computation of the stress concentration for equation 5. The simplest approach is a conservative one. It consists in determining the stress concentration factors independently, as the ratio of the peak stress in the notched specimen to the applied remote stress, for each component. Since the principal stress directions match the reference axes of the model, there is no need for $K_{t\theta z}$ in this particular case. This approach is conservative because it takes into account the point of highest stress for each component, although this point may change for each case. Results for the roll perforations array, shown in figure 8, illustrate the abovementioned effect. The direct approach yields $K_{t\theta} = 3.20$ and $K_{tz} = 3.02$, for different locations as shown in figure 6(a) and 6(b). These stress concentration factors are most conservative when the actual stress state is the one shown in figure 6(c).

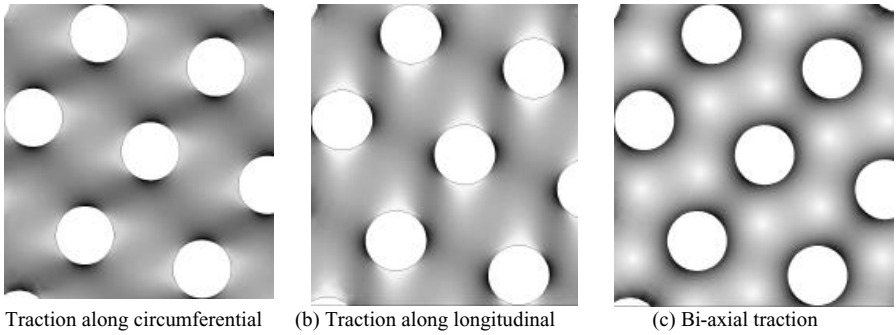

(a) Traction along circumferential axis.

$S_\theta = 1, S_z = 0$

$K_{t\theta} = 3.20$

(b) Traction along longitudinal axis.

$S_\theta = 0, S_z = 1$

$K_{tz} = 3.02$

(c) Bi-axial traction

$S_\theta = 1, S_z = 1$

$K_{t\theta} = 1.69$

$K_{tz} = 1.71$

Figure 6: Theoretical concentration factors for perforated roll. Maximum principal stresses.

Instead of the conservative approach, stress concentrators were computed at the most unfavourable location from the results of the finite elements model, with the actual extremes in the load cycle as boundary conditions. These extremes were found by examining the results from the shell finite elements model of the roll, taking into consideration that traction stresses along the circumferential axis and compressive stresses along the longitudinal axis produce traction stresses at the most unfavourable location. The two extreme conditions are indicated in table 2. The results of the plane stress finite elements model are shown in figure 7.

Table 2: Extreme conditions, results from shell finite elements model of roll.

	Condition 1	Condition 2
$\sigma_{\theta,fem}$ MPa	16.9	-13.1
$\sigma_{z,fem}$ MPa	-1.60	-11.1
$\sigma_{eq,fem}$ MPa	17.75	12.22

The stress concentrators were computed as follows

$$\begin{bmatrix} \sigma_{\theta,1} & \sigma_{z,1} \\ \sigma_{\theta,2} & \sigma_{z,2} \end{bmatrix} \begin{bmatrix} K_{\theta,fem} \\ K_{z,fem} \end{bmatrix} = \begin{bmatrix} \sigma_{1,\max} \\ \sigma_{2,\min} \end{bmatrix}$$
$$\begin{bmatrix} 16.9 & -1.60 \\ -13.1 & -11.1 \end{bmatrix} \begin{bmatrix} K_{\theta,fem} \\ K_{z,fem} \end{bmatrix} = \begin{bmatrix} 79.8 \\ -36.1 \end{bmatrix} \quad (9)$$

$$\begin{bmatrix} K_{\theta,fem} \\ K_{z,fem} \end{bmatrix} = \begin{bmatrix} 4.52 \\ -2.08 \end{bmatrix}$$

From equation 7, the theoretical stress concentrators are

$$K_{t,\theta} = 3.16 \qquad (10)$$
$$K_{t,z} = -1.46$$

The area reduction factor, K_a, was applied to the results for the extreme conditions to obtain true nominal stresses. These were used to compute the mean stress and cyclic nominal stress amplitude for both the circumferential and longitudinal directions. The resulting data is summarized in table 3.

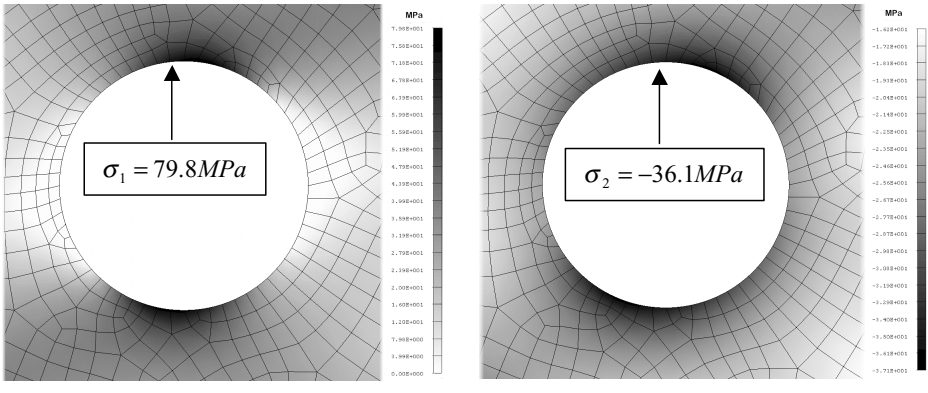

(a) Condition 1. Maximum principal stresses (b) Condition 2. Minimum principal stresses

Fig. 7. Results of plane stress finite elements model

Table 3: Fatigue stress data for extreme conditions

	σ_θ MPa	σ_z Mpa	$\sigma_{\theta,a}$ MPa	$\sigma_{\theta,m}$ MPa	$\sigma_{z,a}$ MPa	$\sigma_{z,m}$ MPa
Condition 1	24.17	-2.29	21.45	2.72	-6.79	-9.08
Condition 2	-18.73	-15.83				

The results of the shell finite elements model indicate that $\sigma_\theta = \sigma_1$ and $\sigma_z = \sigma_2$, with $\tau_{\theta z} = 0$. Thus, equations (2) and (4) can be used to find $\sigma_{a,e}$ and $\sigma_{m,e}$. Note that the directions of the principal stresses actually change as the roll rotates but they are assumed fixed and equal to those corresponding to condition 1.

$$\sigma_{a,e} = \sqrt{\frac{1}{2}\left[(21.45-(-6.77))^2 + 21.45^2 + (-6.77)^2\right]} \tag{11}$$

$$\sigma_{a,e} = 25.53$$

$$\sigma_{m,e} = 2.72 + (-9.08) \tag{12}$$

$$\sigma_{m,e} = -6.36$$

From equation 5, the theoretical stress concentration factor is

$$K_t \cdot 25.52 = \sqrt{\frac{1}{2}\left[(3.16 \cdot 21.45 - (-1.46)\cdot(-6.79))^2 + 3.16^2 \cdot 21.45^2 + (-1.45)^2 \cdot 6.77^2 + 0\right]} \tag{13}$$

$$K_t = 2.49$$

Equation 8 yields the fatigue notch factor

$$K_f = 1 + \frac{2.49-1}{1+\sqrt{\frac{0.2}{2}}} \tag{14}$$

$$K_f = 2.13$$

The fatigue limit of the roll shell, σ_f, is expressed by the following empirical correlation

$$\sigma_f = k_a k_b k_c \sigma_f' \tag{15}$$

where σ_f' is the fatigue limit on the standard specimen and k_a, k_b and k_c are modification factors defined as follows: k_a-loading mode factor; k_b-size effect factor; and k_c-surface roughness factor.

Loading mode factor:

For bending $k_a = 1$

Size effect factor:

For equivalent diameters larger than 50mm [1] $k_b = 0.85$

Surface roughness:

For a 680 MPa tensile strength steel machined surface [1] $k_c = 0.80$

Hence, the modified fatigue limit is

$$\sigma_f = 122.4\ MPa \tag{16}$$

3.2 Fatigue strength reliability

The fatigue strength for the shell material 3RE60 SRG is 180Mpa. This is based on 10^7 load-cycles and a 50% percent probability of failure. As proposed by Mischke[6], a normal distribution is considered for the fatigue limit, with a standard deviation σ equal to 8 percent of the standard fatigue limit (180 MPa). Figure 8 shows the probability of failure of the roll shell material.

The multiple perforations on the perforated shell raise questions about the reliability of the fatigue limit of the part. A simple safety factor on equation 1 may not be able to take into account the variability of the fatigue strength. Since the fatigue limit varies among several fatigue tests, the same variation is expected on the time to the appearance of visible cracks on the perforations.

The amount of possible crack initiation sites in this problem is substantial. From the stress results shown in Fig. 4, it was determined that a 1m long segment of the shell is subject to stresses within a 0.5% of the mid-section values. This segment contains 58,065 perforations.

The reliability of a machine part is defined as

$$F = 1 - P \tag{17}$$

where P is the probability of failure. For a part with N notches, each having a P'probability of failure, the global reliability is

$$F_p = (1 - P')^N \tag{18}$$

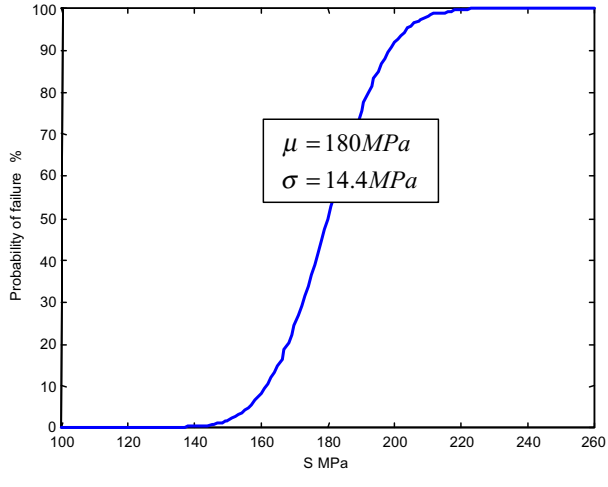

Figure 8: Cumulative frequency plot. Probability P versus stress S, 10^7 cycles.

A 90 percent reliability is specified for the roll. From equation 18, the required probability of failure for each perforation is

$$P' = 1.81^{-6} \tag{19}$$

From Fig.8, the cyclic stress amplitude that yields the requested P'is

$$\sigma_f'' = 113.4\,MPa \tag{20}$$

The reliability factor k_d is defined as

$$k_d = \frac{\sigma_f''}{\sigma_f'} \tag{21}$$

It follows that for the specific case of the roll shell

$$k_d = 0.63 \tag{22}$$

Hence, the fatigue limit of equation 17, modified by k_d to obtain a 90 percent reliability with 58,065 notches is

$$\sigma_{f,r} = 77.1\ MPa \tag{23}$$

3.3 Fatigue life safety factor

The fatigue life safety factor, for infinite life, is obtained from equation1.

$$\frac{1}{N} = \frac{-6.34}{680} + 2.13\frac{25.52}{77.1} \tag{24}$$
$$N = 1.44$$

4 UNCERTAINTY ESTIMATION

The calculated fatigue life safety factor, equation 24, is subject to uncertainties from applied loads, stress values, material properties and modification factors. Since loads are controlled in the paper production process, they are assumed constant. The variability of the material properties is accounted for in the reliability analysis. Correction factors are indeed a potential source of error, since they extend test results performed to specimens in load conditions quite different to those of the real part. A 5% uncertainty is assumed for k_a, k_b and k_c.

Assuming that the individual variables, X_i, are uncorrelated and random[i], the uncertainty in the calculated quantity, Y, can be determined[7] as

$$U_r = \sqrt{\sum_i \left(\frac{\partial Y}{\partial X_i}\right)^2 U_{X_i}^2} \tag{25}$$

[i] This may not actually be the case for different components of the stress tensor at a given location. Although, regarding them as uncorrelated takes into account the fact that the error may differ among components.

where U are the represents the uncertainty of the variable.

Partial derivatives for equation 24 were computed from equations 9 through 24, yielding the following results

$$\frac{\partial N}{\partial k_a}=1.457 \quad \frac{\partial N}{\partial k_b}=1.714 \quad \frac{\partial N}{\partial k_c}=1.821$$
$$\frac{\partial N}{\partial \sigma_{1,\max}}=-0.0138 \quad \frac{\partial N}{\partial \sigma_{21,\min}}=0.00052$$
$$\frac{\partial N}{\partial \sigma_{\theta 1}}=0.0102 \quad \frac{\partial N}{\partial \sigma_{\theta 2}}=0.0240 \quad \frac{\partial N}{\partial \sigma_{z1}}=-0.0261 \quad \frac{\partial N}{\partial \sigma_{z2}}=0.0039 \tag{26}$$

A maximum uncertainty of 10% for the fatigue life safety factor, N, was specified. In order to solve equation 24 for the maximum allowable uncertainties on the stress results, additional constraints must be introduced. Allowing the same relative uncertainty in all five stress results yields the following results

$$N=1.437\pm 0.144 \quad \sigma_{1,\max}=79.8\pm 4.79\,MPa \quad \sigma_{2,\min}=-36.1\pm 2.17\,MPa$$
$$\sigma_{\theta 1}=16.9\pm 1.01\,MPa \quad \sigma_{z1}=-1.6\pm 0.09\,MPa$$
$$\sigma_{\theta 2}=-13.1\pm 0.79\,MPa \quad \sigma_{z2}=-11.1\pm 0.67\,MPa \tag{27}$$

Thus, a maximum 6 percent relative uncertainty is allowable on all finite element stress results to ensure a maximum 10 percent uncertainty on the computed fatigue life safety factor. This condition was met via successive refinement of the finite element meshes.

4.1 Shell finite element model

An initial mesh with 2264 second order shell elements was used. Then, a second mesh was constructed with higher element density in the nip area, where the stresses are highest. The results differed in less than 0.1% between these two meshes. Also, averaged and non-averaged results differed less than 0.01% with the final mesh shown in figure 2. These results and the fact that stress gradients where low lead to the conclusion that the solution has converged well within the required 6 percent error.

4.2 Plane stress finite element model

Accurately computing stress concentrators around holes requires a certain degree of refinement on the mesh. There are methods to estimate the global and local error on a finite element solution and to perform automatic refinement [3] based on these results. Those methods are not suitable to this problem, because automatic refinement tools would refine the mesh around all perforations, resulting in an unnecessarily computer-intensive problem. Instead, local refinement around one perforation was specified, and successive refinement steps

were used to ensure the convergence of the solution.

The refinement scheme is shown in Fig. 11. 60 elements where specified surrounding the central perforation, half that amount (30) on the surrounding perforations and a 2.5mm element length was specified elsewhere. Several meshes were constructed with first and second order finite elements. The general element length was kept constant, varying only the number of elements on the central perforation (from 20 to 200) and surrounding perforations. Results for the non-averaged maximum principal stress at the most unfavourable location are shown in Fig. 10. It is clear that the solution converges to a value of 79.9Mpa. By assuming this value as the real stress, the 6 percent uncertainty limit (dashed line in Fig. 12) is 75.1 MPa. Therefore, stress results obtained with the initial mesh (60 elements on perforation edge) are well within the required uncertainty limit.

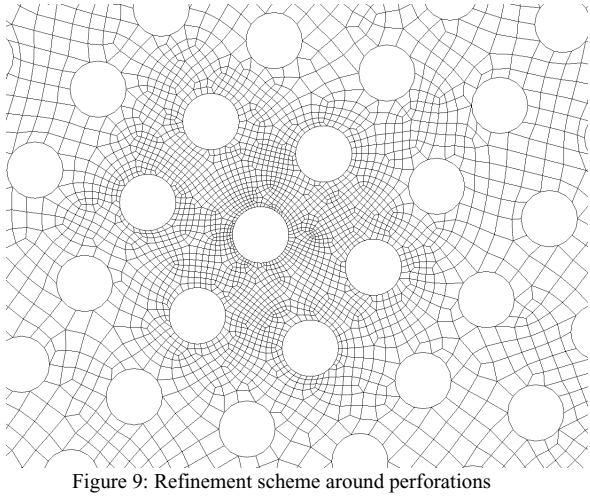

Figure 9: Refinement scheme around perforations

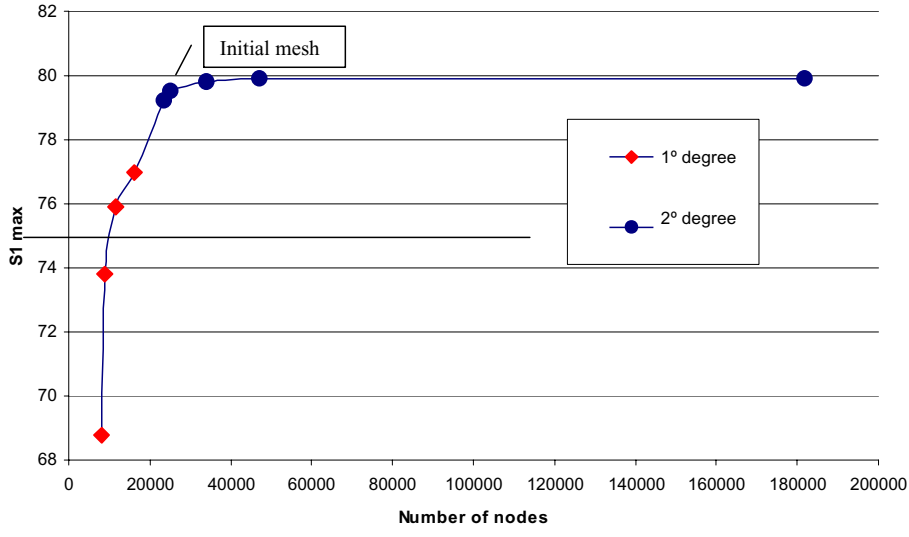

Figure 10: Finite element model solution convergence. Maximum principal stress at critical location.

5 CONCLUSIONS

The presented procedure is an example of engineering analysis with finite element modelling as a valuable tool. The following considerations are noteworthy:

A two-model approach was chosen

The rotating roll was modelled with a static load-case instead of defining complex time-varying load functions on the shell surface

Fatigue stress concentrators were carefully computed. An area reduction factor had to be introduced in order to quantify the stress gradient near perforations

Judicious mesh refining saves computing time

The mayor factors affecting the predicted fatigue life are stress concentrators on the roll shell and the loss of reliability due to the high amount of notches.

The uncertainty analysis yields interesting conclusions. The infinite fatigue life safety factor is not as sensitive to stress results as expected. Although the precision of finite element results is an important issue, the required acc uracy for this problem was met with ease.

6 REFERENCES

[1] Zahavi, E and Torbilo, V. 1996. *Life expectancy of machine parts: fatigue design*. CRC Press.

[2] Sines, G and G.L. Waisman. 1959. *Behaviour of Metals under Complex Static and Alternating Stresses, in Metal Fatigue*. New York: McGraw-Hill, 197.

[3] Fuchs, H.O. and R.I. Stephens. 1980. *Metal Fatigue in Engineering*. New York: John Wiley.

[4] Neubert, H. *Theory of Notch Stresses, Principles and Exact Calculations*, Edwards, Ann Arbor, Michigan, 1946.

[5] Grover, H., *Fatigue of Metals and Structures*, NAVWEPS 00-25-534, Washington, 1960.

[6] Mischke, C. 1974. *A rationale for mechanical design to a reliability specification*. ASME Design Engineering Technical Conference, New York.

[7] Taylor B.N. and Kuyatt, C.E. *Guidelines for Evaluating and Expressing the Uncertainty of NIST Measurement Results*, National Institute of Standards and Technology Technical Note 1297, 1994.